AIP | The Journal of Chemical Physics

Membrane curvature generated by asymmetric depletion layers of ions, small molecules, and nanoparticles

Bartosz Różycki and Reinhard Lipowsky

Citation: The Journal of Chemical Physics **145**, 074117 (2016); doi: 10.1063/1.4960772
View online: http://dx.doi.org/10.1063/1.4960772
View Table of Contents: http://scitation.aip.org/content/aip/journal/jcp/145/7?ver=pdfcov
Published by the AIP Publishing

Membrane curvature generated by asymmetric depletion layers of ions, small molecules, and nanoparticles

Bartosz Różycki[1] and Reinhard Lipowsky[2,a),b)]
[1]*Institute of Physics, Polish Academy of Sciences, Aleja Lotników 32/46, 02-668 Warsaw, Poland*
[2]*Department of Theory & Biosystems, Max Planck Institute of Colloids and Interfaces, 14424 Potsdam, Germany*

(Received 28 March 2016; accepted 18 July 2016; published online 19 August 2016)

Biomimetic and biological membranes consist of molecular bilayers with two leaflets that are typically exposed to different aqueous solutions. We consider solutions of "particles" that experience effectively repulsive interactions with these membranes and form depletion layers in front of the membrane leaflets. The particles considered here are water-soluble, have a size between a few angstrom and a few nanometers as well as a rigid, more or less globular shape, and do neither adsorb onto the membranes nor permeate these membranes. Examples are provided by ions, small sugar molecules, globular proteins, or inorganic nanoparticles with a hydrophilic surface. We first study depletion layers in a hard-core system based on ideal particle solutions as well as hard-wall interactions between these particles and the membrane. For this system, we obtain exact expressions for the coverages and tensions of the two leaflets as well as for the spontaneous curvature of the bilayer membrane. All of these quantities depend linearly on the particle concentrations. The exact results for the hard-core system also show that the spontaneous curvature can be directly deduced from the planar membrane geometry. Our results for the hard-core system apply both to ions and solutes that are small compared to the membrane thickness and to nanoparticles with a size that is comparable to the membrane thickness, provided the particle solutions are sufficiently dilute. We then corroborate the different relationships found for the hard-core system by extensive simulations of a soft-core particle system using dissipative particle dynamics. The simulations confirm the linear relationships obtained for the hard-core system. Both our analytical and our simulation results show that the spontaneous curvature induced by a single particle species can be quite large. When one leaflet of the membrane is exposed, e.g., to a 100 mM solution of glucose, a lipid bilayer can acquire a spontaneous curvature of $\pm 1/(270\ \text{nm})$. Our theoretical results can be scrutinized by systematic experimental studies using a large variety of different types of particles. [http://dx.doi.org/10.1063/1.4960772]

I. INTRODUCTION

Biological and biomimetic membranes consist of bilayers with two leaflets of lipid molecules. If such a membrane is exposed to "particles" that experience effectively repulsive interactions with the membrane, the particles are excluded from the membrane and form depletion layers in front of the two leaflets as illustrated in Fig. 1. When the two depletion layers differ in their physico-chemical properties, the membrane becomes asymmetric and prefers to adopt a certain spontaneous curvature.[1,2] In this paper, we corroborate this depletion-induced curvature both for a hard-core and for a soft-core system using analytical methods and molecular simulations. The simulations extend our recent study in which we determined the membrane curvature arising from asymmetric adsorption layers.[3]

Depletion effects are well understood for solutions of particles with different sizes. Each particle occupies a certain volume from which other particles are excluded. The exclusion of the smaller particles by the larger ones leads to an effective attraction between the larger particles because the smaller particles gain translational entropy when the larger ones move closer together.[4] As a result of the effectively attractive interactions, the particle mixture can undergo phase separation.[5] These depletion effects have been studied in some detail, both theoretically[6–9] and experimentally,[10,11] see the review in Ref. 12.

Membrane curvature generated by asymmetric depletion layers as depicted in Fig. 1 represents another depletion effect, arising from the interplay between excluded volume and membrane flexibility. Indeed, for each depletion layer, the translational entropy loss of the particles depends on the volume of this layer and on the particle concentration in the adjacent solution. Therefore, the membrane prefers to curve in such a way that it reduces the number of excluded particles. If the system contains only a single particle species, the total number of excluded particles is reduced when the membrane bulges (or curves) towards the solution with the smaller particle concentration as shown in Fig. 1(a). If the

a)Electronic mail: lipowsky@mpikg.mpg.de
b)URL: http://www.mpg.mpikg.de/th.

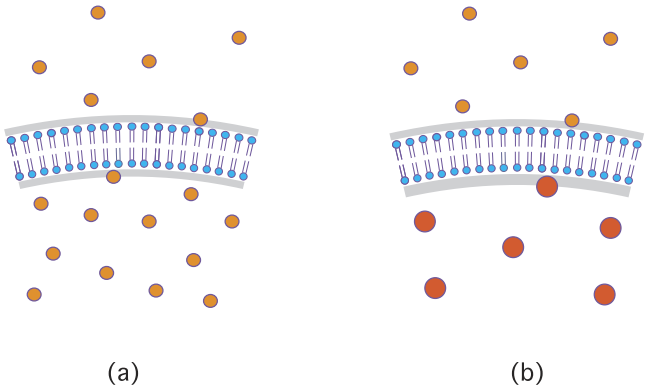

FIG. 1. Spontaneous (or preferred) curvature of bilayer membranes (blue) as generated by depletion layers (light grey) in front of the two membrane-water interfaces: (a) The exterior and the interior solution contain different molar concentrations of the same particle species and (b) the interior and the exterior solution contain the same molar concentration of two different particle species. In (a) and (b), the membrane bulges (or curves) towards the solution with the smaller particle concentration and the smaller particle size, respectively. In both cases, the preferred curvature reduces the number of particles excluded from the two depletion layers and, thus, the associated loss of translational entropy.

exterior and the interior solution contain the same molar concentration of two distinct particle species, the membrane bulges preferentially towards the solution with the smaller particle size, see Fig. 1(b).

The particles considered here are water-soluble, have a size between a few angstrom and a few nanometers, as well as a rigid and more or less globular shape. Because of their effectively repulsive interactions with the membranes, the particles do neither adsorb onto nor permeate through these membranes. Examples for such particles are provided by ions,[13] small sugar molecules,[14] short PEG chains,[15] globular proteins, functionalized dendrimers, or inorganic nanoparticles with a hydrophilic surface. In all cases, we will focus on the loss of translational entropy and will not include additional internal degrees of freedom. In particular, we will not include the loss of configurational entropy that long flexible polymers[7,9,16,17] or rod-like molecules[18,19] suffer adjacent to a membrane surface.

As shown below, the depletion layers formed by the particles lead to leaflet coverages and leaflet tensions of the bilayer membranes that are proportional to the particle concentrations in the aqueous solutions and to spontaneous curvatures that are proportional to the concentration differences across the membranes. These simple linear dependencies are obtained for both hard-core and soft-core interactions between the particles. The leaflet coverages are negative and decrease with increasing particle concentrations whereas the leaflet tensions increase with these concentrations. Symmetric depletion layers are obtained if the two leaflets are exposed to the same aqueous solution. In this case, we focus on bilayers that are compressed in the absence of the particles and determine the "critical" particle concentration for which the membrane becomes tensionless. Asymmetric depletion layers are obtained if the two leaflets are exposed to different aqueous solutions. In the latter case, the membrane acquires a preferred or spontaneous curvature that is proportional to the difference in the particle concentrations of the two aqueous solutions. The spontaneous curvature induced by the depletion layers of a single particle species can be quite large. As an example, consider a lipid bilayer that has the bending rigidity $\kappa = 20\ k_BT$ and is exposed, on one side, to a 100 mM glucose solution. When we model the glucose molecules as spherical particles with a diameter of 1 nm, we obtain a depletion-induced spontaneous curvature of about $\pm 1/(270\ \text{nm})$.

Our paper is organized as follows. We first consider a hard-core system for which the depletion-induced spontaneous curvature can be obtained analytically. This system is characterized by linear dependencies of the leaflet coverages and leaflet tensions on the particle concentrations in the adjacent aqueous solutions. Furthermore, the hard-core system leads to a spontaneous curvature that is proportional to the difference between the particle concentrations on the two sides of the membrane. In Sec. III, we describe our computational method based on Dissipative Particle Dynamics (DPD). The latter method involves soft-core particles for which we propose linear relationships in close analogy to the hard-core system. These relationships are then confirmed by the simulations in Secs. IV and V, both for symmetric and asymmetric bilayers. At the end, we discuss the simulation results and give a short summary and outlook.

II. SPONTANEOUS CURVATURE GENERATED BY DEPLETION LAYERS IN A HARD-CORE SYSTEM

We first study a reference system for which the depletion-induced spontaneous curvature can be obtained analytically.[1] This system is based on ideal particle solutions and hard-core interactions between these particles and the membrane. The latter system involves only two parameters apart from the membrane's bending rigidity: the membrane thickness and the particle size. The nanoparticles are taken to be spherical with a hard-core radius R_{hc}, and the bilayer is described as a thin film bounded by two impenetrable membrane-water interfaces with constant separation ℓ_{hw} (the subscript "hw" stands for "hard wall").

The bilayer membrane separates the aqueous medium into two compartments, an exterior and an interior one, which are in contact with the outer and the inner leaflet of the bilayer. In the absence of the nanoparticles, the membrane is taken to be symmetric. The membrane tension Σ_{no} is then equally shared by both leaflets and each leaflet experiences the tension

$$\Sigma_l = \frac{1}{2}\,\Sigma_{\text{no}} \quad \text{(no particles)} \tag{1}$$

with the subscript l = 'ex' or 'in' corresponding to the outer or inner leaflet, respectively. In general, the "bare" tension Σ_{no} reflects external forces or constraints. In the molecular dynamics simulations described below, this tension arises from the periodic boundary conditions and the chosen size of the simulation box which together determine the projected membrane area per lipid molecule.[3,20,21]

A. Excess tensions and negative coverages of leaflets

We now disperse nanoparticles in the two aqueous compartments and characterize these compartments by their molar particle concentrations, $X_{\rm ex}$ and $X_{\rm in}$. The bilayer is then exposed to a symmetric and asymmetric environment for $X_{\rm ex} = X_{\rm in}$ and $X_{\rm ex} \neq X_{\rm in}$, respectively. The repulsive interactions between the particles and the membrane lead to depletion layers close to the two leaflets of the bilayer. The volumes of these depletion layers, $\Omega_{\rm ex}$ and $\Omega_{\rm in}$, depend on the membrane geometry. In the dilute limit in which we can ignore particle-particle interactions, the excess free energies $\delta F_{\rm ex}$ and $\delta F_{\rm in}$ arising from the depletion layers have the form[1]

$$\delta F_l = k_{\rm B}T\, X_l\, \Omega_l \quad \text{for large particle numbers} \tag{2}$$

with $l = {\rm ex}, {\rm in}$ (which now plays the role of a leaflet or layer index). The expression for δF_l as given by Eq. (2) is obtained for an ideal solution of particles and applies to any shape of the membrane. The scale for the excess free energies δF_l is set by the thermal energy $k_{\rm B}T$ which reflects the entropic origin of these free energies.

For a laterally uniform membrane, the excess free energies δF_l are proportional to the area A of the midsurface between the two leaflets of the bilayer. The midsurface provides a common reference surface for both leaflets. In a curved state, the areas $A_{\rm ex}$ and $A_{\rm in}$ of the two leaflet-water interfaces differ from the area A of the midsurface but are proportional to A, see further below. Therefore, we define the excess tensions $\delta\Sigma_l$ of the two leaflets by

$$\delta\Sigma_l \equiv \frac{\delta F_l}{A} = k_{\rm B}T\, X_l\, \frac{\Omega_l}{A}. \tag{3}$$

The overall tension of leaflet l is then given by

$$\Sigma_l = \frac{1}{2}\,\Sigma_{\rm no} + \delta\Sigma_l. \tag{4}$$

It follows from Eq. (3) that the excess tension $\delta\Sigma_l$ must be positive but the leaflet tension $\frac{1}{2}\,\Sigma_{\rm no}$ arising from external forces or constraints for $X_{\rm ex} = X_{\rm in} = 0$ can be positive or negative. Therefore, the two terms in Eq. (4) may cancel each other, leading to a tensionless state with $\Sigma_l = 0$.

The number of particles excluded from depletion layer l is $X_l\Omega_l$ which implies the *negative* coverage

$$\Gamma_l \equiv -\frac{X_l\Omega_l}{A} \tag{5}$$

of leaflet l. Note that the leaflet tensions Σ_l and the coverages Γ_l satisfy the relations

$$\frac{\partial\,\Sigma_l}{\partial X_l} = \frac{\partial\,\delta\Sigma_l}{\partial X_l} = -k_{\rm B}T\,\frac{\Gamma_l}{X_l} \tag{6}$$

which have the same form as the Gibbs adsorption equation for macroscopic interfaces. Furthermore, for the ideal particle solution considered here, we also have the simple relationship

$$\delta\Sigma_l = -k_{\rm B}T\,\Gamma_l \tag{7}$$

between the excess tensions and the coverages. The relations (3)-(7) again apply to any shape of the membrane. In Subsections II B–II C, we will consider three particularly simple shapes: a planar membrane, a cylindrical membrane tube, and a spherical membrane cap.

B. Planar membrane

The simplest geometry is provided by a planar membrane. In this case, the area A of the bilayer's midplane is equal to the areas $A_{\rm ex}$ and $A_{\rm in}$ of the outer and the inner membrane-water interface. Furthermore, the volumes of the two depletion layers are identical and given by $\Omega_{\rm in}^{\rm pl} = \Omega_{\rm ex}^{\rm pl} = AR_{\rm hc}$.

We introduce the Cartesian coordinate z perpendicular to the membrane and place the two membrane-water interfaces at $z = z_{\rm ex} \equiv \frac{1}{2}\,\ell_{\rm hw}$ and $z = z_{\rm in} \equiv -\frac{1}{2}\,\ell_{\rm hw}$. The subscript "hw" indicates that we consider these surfaces as "hard walls" which are impenetrable to the particles. We use the convention that the subvolumes with $z > z_{\rm ex}$ and $z < z_{\rm in}$ contain the exterior and interior solution, respectively. Because of the planar geometry, the particle number density $\rho_{\rm P}$ depends only on the coordinate z. The resulting density profile $\rho_{\rm P}(z)$ determines the coverages $\Gamma_{\rm ex}$ and $\Gamma_{\rm in}$ of the outer and inner leaflets via

$$\Gamma_{\rm ex}^{\rm pl} \equiv \int_{z_{\rm ex}}^{\infty} dz[\rho_{\rm P}(z) - X_{\rm ex}] = -R_{\rm hc}X_{\rm ex} \tag{8}$$

and

$$\Gamma_{\rm in}^{\rm pl} \equiv \int_{-\infty}^{z_{\rm in}} dz[\rho_{\rm P}(z) - X_{\rm in}] = -R_{\rm hc}X_{\rm in}. \tag{9}$$

The same coverages are obtained when we specify the general expression (5) to the planar case.

Likewise, the expression for the excess tensions $\delta\Sigma_l$ as given by Eq. (7) leads to

$$\delta\Sigma_l = \delta\Sigma_l^{\rm pl} \equiv k_{\rm B}T\, R_{\rm hc}\, X_l \tag{10}$$

for the planar geometry.

C. Curvature expansion of excess tensions and coverages

Next, we consider a cylindrical membrane tube formed by a bilayer of thickness $\ell_{\rm hw}$. We now need to distinguish three cylindrical surfaces: the outer membrane-water surface with area $A_{\rm ex}$, the inner membrane-water surface with area $A_{\rm in}$, and the midsurface with area A. This midsurface has the curvature radius $R_{\rm cy}$ which defines the mean curvature $M = 1/(2R_{\rm cy})$ of the cylindrical membrane tube.

Because of the cylindrical geometry, the areas $A_{\rm ex}$ and $A_{\rm in}$ of the two membrane-water interfaces are related to the area A of the midsurface via

$$A_l \approx A(1 + s_l\,\ell_{\rm hw}M) \quad \text{for } l = {\rm ex}, {\rm in} \tag{11}$$

up to first order in the mean curvature M with the sign function

$$\begin{aligned} s_l &\equiv +1 \quad \text{for } l = {\rm ex} \\ &\equiv -1 \quad \text{for } l = {\rm in}. \end{aligned}$$

Here and below, the symbol "≈" stands for "asymptotically equal," i.e., equal in the limit in which a certain parameter becomes small or large. The excluded volumes $\Omega_{\rm ex}$ and $\Omega_{\rm in}$ in front of the two bilayer leaflets are then given by

$$\Omega_l \approx A\,R_{\rm hc}[1 + s_l\,(\ell_{\rm hw} + R_{\rm hc})M] \tag{12}$$

up to first order in M. Note that Ω_l is approximately but not exactly equal to $A_l R_{\rm hc}$.

Using the general expressions (5) for the coverage and (3) for the excess tension, we obtain the negative coverage

$$\Gamma_l \approx -R_{\rm hc}\,[1 + s_l(\ell_{\rm hw} + R_{\rm hc})M]\,X_l \tag{13}$$

and the excess tension

$$\delta\Sigma_l \approx k_{\rm B}TR_{\rm hc}\,[1 + s_l\,(\ell_{\rm hw} + R_{\rm hc})M]\,X_l \tag{14}$$

of leaflet l.

The same line of reasoning can also be applied to a spherical membrane cap. The radius $R_{\rm sp}$ of the midsurface now defines the mean curvature $M = 1/R_{\rm sp}$ of the membrane. To first order in M, we then obtain the same M-dependence for the coverages and for the excess tensions as for the cylindrical membrane tube.

D. Bilayer tension

The expression for the leaflet excess tensions as given by Eq. (14) implies that the bilayer tension has the form

$$\Sigma = \Sigma_{\rm no} + \delta\Sigma_{\rm ex} + \delta\Sigma_{\rm in} = \Sigma_{\rm no} + \delta\Sigma^{\rm pl} + \zeta M \tag{15}$$

up to first order in M with the excess tension

$$\delta\Sigma^{\rm pl} \equiv k_{\rm B}TR_{\rm hc}(X_{\rm ex} + X_{\rm in}) \tag{16}$$

of the planar membrane and the asymmetry coefficient

$$\zeta \equiv k_{\rm B}TR_{\rm hc}(\ell_{\rm hw} + R_{\rm hc})(X_{\rm ex} - X_{\rm in}). \tag{17}$$

For a symmetric environment with $X_{\rm ex} = X_{\rm in} = X$, the asymmetry coefficient ζ vanishes and the bilayer tension becomes

$$\Sigma = \Sigma_{\rm no} + \delta\Sigma^{\rm pl} = \Sigma_{\rm no} + 2k_{\rm B}TR_{\rm hc}\,X. \tag{18}$$

For an asymmetric environment with $X_{\rm ex} \neq X_{\rm in}$, the depletion layers generate a spontaneous curvature as described in Subsection II E.

E. Spontaneous curvature induced by depletion layers

The spontaneous curvature, m, can be obtained by identifying the term of order M in the relation (15) with the corresponding term, $-4\kappa mM$, of the bending energy in the spontaneous curvature model[22,23] which also involves the bending rigidity κ of the membrane. This identification leads to[1]

$$m = -\frac{\zeta}{4\kappa} = \frac{k_{\rm B}T}{4\kappa}R_{\rm hc}(\ell_{\rm hw} + R_{\rm hc})(X_{\rm in} - X_{\rm ex}). \tag{19}$$

Thus, the spontaneous curvature m is positive if the particle concentration $X_{\rm in}$ in the interior solution is larger than the particle concentration $X_{\rm ex}$ in the exterior solution but negative for $X_{\rm ex} > X_{\rm in}$, see Fig. 1(a). As a consequence, for particle depletion, the membrane prefers to bulge (or curve) towards the aqueous solution with the smaller particle density. In contrast, for particle adsorption, the membrane prefers to bulge towards the aqueous compartment with the larger particle density.[1,3]

F. Dilute particle solutions

It is interesting to note that the derivation of Eq. (19) did not involve any assumption about the relative size of the particle radius $R_{\rm hc}$ and the membrane thickness $\ell_{\rm hw}$. Thus, as long as the solution is sufficiently dilute so that we can neglect particle-particle interactions, the expression (19) will also apply for particle radii that are comparable or even larger than the membrane thickness.

A simple criterion for a dilute solution of hard spheres with diameter $d_{\rm hc} = 2R_{\rm hc}$ is obtained from the virial expansion which leads to the equation of state

$$P \approx k_{\rm B}TX(1 + B_2X) \quad \text{with} \quad B_2 \equiv 2\pi d_{\rm hc}^3/3 \tag{20}$$

up to second order in X. The ideal gas description provides a reasonable approximation as long as the leading term is large compared to the correction term of order X^2 or, equivalently, when the molar concentration X is small compared to the crossover concentration

$$X_o \equiv \frac{1}{B_2} = \frac{3}{2\pi d_{\rm hc}^3} = \frac{0.478}{d_{\rm hc}^3}. \tag{21}$$

As we increase the particle concentration beyond X_o, the hard spheres start to freeze at the concentration $X = X_{\rm fr}$ with $X_{\rm fr} = 0.944/d_{\rm hc}^3 \simeq 2X_o$ corresponding to a volume (or packing) fraction of 0.494.[24]

In Table I, we provide numerical values for the crossover concentration X_o for a few particle sizes of interest. In addition, we also include values for the inverse spontaneous curvature $1/m$ as obtained from Eq. (19) for particle concentrations $X_{\rm in} = X_o$ and $X_{\rm ex} = 0$, using the typical value $\kappa = 10^{-19}$ J for the bending rigidity of lipid bilayers. Inspection of the $(1/m)$-values in Table I shows that the spontaneous curvature m induced by the particle concentration X_o decreases rapidly with increasing particle size.

G. Several species of particles

It has been tacitly assumed here that the exterior and interior solutions are osmotically balanced. This balance may involve a second "neutral" particle species that is neither depleted from nor adsorbed to the membrane corresponding to constant density profiles of these particles. Alternatively, one may consider two or more different particle species as in Ref. 1 and illustrated in Fig. 1(b). In general, let us consider an arbitrary number of different particle species distinguished

TABLE I. Radii $R_{\rm hc}$ and diameters $d_{\rm hc}$ of hard spheres, corresponding crossover concentrations X_o as defined by Eq. (21) in units of 1/nm^3 and M (moles/dm^3), and inverse spontaneous curvature $1/m$ as obtained from Eq. (19) for particle concentrations $X_{\rm in} = X_o$ and $X_{\rm ex} = 0$ as well as bending rigidity $\kappa = 10^{-19}$ J.

$R_{\rm hc}$ (nm)	0.25	0.5	1	1.5	2
$d_{\rm hc}$ (nm)	0.5	1	2	3	4
X_o (1/nm^3)	3.8	0.48	0.06	0.02	0.008
X_o (M)	6.3	0.80	0.10	0.03	0.01
$1/m$ (nm)	20	73	266	536	1107

by the subscript j. The species j then makes the contribution[1]

$$m_j = -\frac{\zeta}{4\kappa} = \frac{k_B T}{4\kappa} R_{hc,j}(\ell_{hw} + R_{hc,j})(X_{in,j} - X_{ex,j}) \quad (22)$$

to the spontaneous curvature and the total spontaneous curvature becomes

$$m = \sum_j m_j. \quad (23)$$

Furthermore, the osmotic balance implies the additional constraint

$$\sum_j (X_{in,j} - X_{ex,j}) = 0 \quad (24)$$

on the particle concentrations.

H. Spontaneous curvature from planar geometry

The spontaneous curvature as given by Eq. (19) can be rewritten in terms of the leaflet tensions $\delta\Sigma_l^{pl} = k_B T\, R_{hc}\, X_l$ for the *planar* geometry as defined in Eq. (10). We then obtain the relationship

$$m = \frac{1}{4\kappa}(\ell_{hw} + R_{hc})(\delta\Sigma_{in}^{pl} - \delta\Sigma_{ex}^{pl}) \quad (25)$$

between the spontaneous curvature m and the excess tensions $\delta\Sigma_{ex}^{pl}$ and $\delta\Sigma_{in}^{in}$ of the planar membrane. Note that the bare tension $\frac{1}{2}\Sigma_{no}$ drops out from the difference $\Sigma_{in}^{pl} - \Sigma_{ex}^{pl}$ of the overall leaflet tensions which is therefore equal to the difference $\delta\Sigma_{in}^{pl} - \delta\Sigma_{ex}^{in}$ of the excess tensions. As a consequence, relationship (25) is equivalent to

$$m = \frac{1}{4\kappa}(\ell_{hw} + R_{hc})(\Sigma_{in}^{pl} - \Sigma_{ex}^{pl}). \quad (26)$$

The expressions as given by Eqs. (25) and (26) show explicitly that the spontaneous curvature m can be obtained from the properties of the *planar* membrane when this membrane is exposed to an *asymmetric* environment. This relationship between the spontaneous curvature and the planar geometry has been emphasized in our previous study on particle adsorption[3] without, however, providing a specific example for which this relationship was proven in a rigorous manner. Depletion layers arising from ideal particle solutions as considered here represent such an example as demonstrated by the exact Eqs. (25) and (26).

I. Tensionless bilayer states

In order to determine the spontaneous curvature for the planar geometry by simulations, it will be convenient to choose a symmetric and tensionless reference state of the bilayer membrane. If the membrane is exposed to a symmetric environment with $X_{ex} = X_{in} = X$, it experiences the bilayer tension

$$\Sigma^{pl} = \Sigma_{no} + k_B T R_{hc} 2X$$

as in Eq. (18) which vanishes for

$$\Sigma_{no} = -k_B T R_{hc} 2X. \quad (27)$$

Therefore, a tensionless state can be obtained for any value of X by an appropriate choice of the bare tension Σ_{no} arising from the external forces and constraints. Because of the minus sign in Eq. (27), this bare tension acts to compress the bilayer. Alternatively, for a given bare tension $\Sigma_{no} < 0$, we obtain a tensionless state for the particle concentration

$$X = X_0 \equiv \frac{|\Sigma_{no}|}{2k_B T R_{hc}}. \quad (28)$$

For the asymmetric case with particle concentrations $X_{ex} \neq X_{in}$, we introduce the excess concentrations

$$Y_{ex} \equiv X_{ex} - X_0 \quad \text{and} \quad Y_{in} \equiv X_{in} - X_0. \quad (29)$$

The bilayer tension now has the form

$$\Sigma^{pl} = \Sigma_{no} + k_B T R_{hc}(2X_0 + Y_{ex} + Y_{in}) \quad (30)$$

which vanishes for

$$Y_{in} = -Y_{ex} \quad \text{or} \quad \frac{1}{2}(X_{ex} + X_{in}) = X_0. \quad (31)$$

Thus, if the planar membrane is symmetric and tensionless for concentration $X_{ex} = X_{in} = X_0$, it is asymmetric and tensionless for any concentration pair, X_{ex} and X_{in}, for which $\frac{1}{2}(X_{ex} + X_{in}) = X_0$.

III. COMPUTATIONAL METHOD

In Secs. IV–V, we will study the depletion-induced spontaneous curvature by Dissipative Particle Dynamics (DPD) simulations of particles with soft-core interactions. In the present section, we briefly review our computational approach, a more detailed account has been given in Refs. 21 and 3.

A. Dissipative particle dynamics

Lipid molecules have a hydrophilic head group and two hydrophobic chains. In our particle-based model, each of the chains consists of six beads of type C and the head group is built up from three beads of type H. The non-adhesive particles are represented by single beads of type P. As in our previous simulation study,[3] we take all beads, including the particle beads, to have the same diameter d, which is convenient from a computational point of view. Furthermore, the separation of the two head group layers is about $5d$. For lipid bilayers, this separation has a typical value of 4 nm which implies that the bead diameter $d \simeq 4\,\text{nm}/5 = 0.8\,\text{nm}$.[3]

The interactions between the DPD beads are parametrized in the usual form,[3,21,25] the corresponding DPD parameters a_{ij} are given in Table II. These parameters describe the strength of the repulsive forces between the soft-core particles.

In our previous work,[3] we studied adsorption of small molecules on lipid bilayers. The adsorbate molecules were simulated as single beads and the lipids had the same molecular architecture as the model lipids in the present study. Furthermore, most of the DPD parameters a_{ij} had the same values except for a_{PH} and a_{PW}, which had the values $a_{PH} = 25k_B T/d$ and $a_{PW} = 35k_B T/d$ in Ref. 3. In the present study, the PH force is more repulsive with $a_{PH} = 40k_B T/d$ whereas the PW force is now less repulsive with $a_{PW} = 25k_B T/d$, see Table II. As we will see below, the

TABLE II. DPD parameters a_{ij}, which describe the strength of the repulsive forces between the soft-core particles, in units of k_BT/d. Here, H, C, W, and P denote the lipid head beads, the lipid chain beads, the water beads, and the non-adhesive particle beads, respectively.

a_{ij}	H	C	W	P
H	30	50	30	40
C	50	10	75	75
W	30	75	25	25
P	40	75	25	25

latter choice of the DPD parameters a_{PH} and a_{PH} leads to depletion layers of the particles in front of the head group layers.

In Ref. 3, we also studied the lipid bilayer in the absence of any particles and obtained the value $\kappa = 15\,k_BT$ for its bending rigidity. The same κ-value applies to the present study because we use the same DPD parameters for the interactions between H, C, and W beads.

In all simulations described below, we used a cuboid simulation box and Cartesian coordinates x, y, and z with periodic boundary conditions in all three directions. The bilayer spans the simulation box parallel to the (x, y)-plane and perpendicular to the z-coordinate. The box contained N_W water beads, N_{Li} lipid molecules, and N_P non-adhesive particles. The mole fraction of the non-adhesive particles is then given by

$$\Phi_P \equiv \frac{N_P}{N_W + N_{Li} + N_P}. \tag{32}$$

B. Particle density profile and extended coverages

Because of the periodic boundary conditions, the particle number density ρ_P depends only on the coordinate z perpendicular to the membrane. The density profile $\rho_P(z)$ determines the particle coverage of the two leaflets as in Eqs. (8) and (9) for the hard-core system. The latter equations involve the locations $\pm\frac{1}{2}\,\ell_{hw}$ of the hard walls corresponding to the membrane-water interfaces. However, for the soft-core interactions used in the DPD simulations, the membrane-water interfaces represent soft rather than hard walls. Therefore, we cannot directly calculate the two leaflet coverages using the hard-core expressions in Eqs. (8) and (9). Instead, we will now consider the extended coverages

$$\tilde{\Gamma}^{pl}_{ex} \equiv \int_0^\infty dz[\rho_P(z) - X_{ex}] \tag{33}$$

and

$$\tilde{\Gamma}^{pl}_{in} \equiv \int_{-\infty}^0 dz[\rho_P(z) - X_{in}] \tag{34}$$

which include the leaflet volumes and can be calculated without any *a priori* knowledge about the locations of the membrane-water interfaces. For a symmetric environment with $X_{ex} = X_{in} = X$, the two extended coverages $\tilde{\Gamma}^{pl}_{ex}$ and $\tilde{\Gamma}^{pl}_{in}$ have the same negative value given by

$$\tilde{\Gamma}^{pl}_{sy} = \frac{1}{2}\int_{-\infty}^{+\infty} dz\,[\rho_P(z) - X]\,, \tag{35}$$

where the subscript sy indicates that this is the coverage on a single leaflet of a symmetric bilayer. For the hard-core system described in Sec. II, the coverage as given by Eq. (35) becomes

$$\tilde{\Gamma}^{pl}_{sy} = -\frac{1}{2}\,(\ell_{hw} + 2R_{hc})X \tag{36}$$

for $l = in, ex$. As shown below, the data of the DPD simulations for the symmetric soft-core system also lead to a linear relationship between the extended coverage and the molar concentration which can be written in the form

$$\tilde{\Gamma}^{pl}_{sy} = -\frac{1}{2}\,(\ell_1 + 2R_1)X, \tag{37}$$

where we have decomposed the proportionality factor into an effective membrane thickness ℓ_1 and an effective particle radius R_1, in close analogy to the hard-core expression (36). In order to determine these two length scales separately, we need a second equation which will be provided by the bilayer tension as explained further below.

C. Stress profile

Both the bilayer tension and the spontaneous curvature of the planar membrane can be obtained from the stress profile across the membrane. Because the aqueous solution and the bilayer membrane are fluid, the pressure tensor is diagonal with the tangential component $P_T = P_{xx} = P_{yy}$ and the normal component $P_N = P_{zz}$. These two components determine the stress profile[20]

$$s(z) = P_N - P_T(z) \tag{38}$$

and the bilayer tension

$$\Sigma^{pl} = \int_{-\infty}^{+\infty} dz\, s(z) \tag{39}$$

acting across the planar membrane.[26] It is useful to decompose this tension into two partial tensions corresponding to the two leaflets of the bilayer. These leaflet tensions are defined by[3]

$$\Sigma^{pl}_{ex} \equiv \int_0^{+\infty} dz\, s(z) \tag{40}$$

and

$$\Sigma^{pl}_{in} \equiv \int_{-\infty}^0 dz\, s(z), \tag{41}$$

where $z = 0$ corresponds to the midplane of the bilayer. Thus, the exterior and interior solutions are again located at $z > 0$ and $z < 0$, respectively.

D. Concentration dependence of bilayer tension

For a symmetric hard-core system, the bilayer tension Σ^{pl} increases linearly with the particle concentration X as in Eq. (18), which implies

$$\frac{\partial \Sigma^{pl}}{\partial X} = 2k_BTR_{hc}. \tag{42}$$

As shown below, the data of the DPD simulations for the soft-core system are well fitted by the linear relation

$$\Sigma^{pl} = \Sigma^{pl}_{no} + 2k_BTR_1\,X \tag{43}$$

which is equivalent to

$$\frac{\partial \Sigma^{\rm pl}}{\partial X} = 2k_{\rm B}TR_1 \tag{44}$$

and defines the effective particle radius R_1 as obtained from the tension and thus from the integrated stress profiles of a symmetric bilayer. Fitting the simulation data for this stress profile and for the particle density profile by the expressions (43) and (37), we obtain the proportionality factors $\ell_1 + 2R_1$ and R_1 and, thus, both the effective particle radius R_1 and the effective membrane thickness ℓ_1.

E. Spontaneous curvature from solution asymmetry

For the asymmetric hard-core system, we also derived a linear relationship between the spontaneous curvature m and the concentration difference $X_{\rm in} - X_{\rm ex}$ as given by Eq. (19) which is equivalent to

$$2\kappa m = \frac{1}{2}\, k_{\rm B}TR_{\rm hc}(\ell_{\rm hw} + R_{\rm hc})(X_{\rm in} - X_{\rm ex}). \tag{45}$$

The simulation data for the soft-core DPD particles presented further below are well fitted by the analogous relationship

$$2\kappa m = \frac{1}{2}\, k_{\rm B}TR_2\,(\ell_2 + R_2)\,(X_{\rm in} - X_{\rm ex}), \tag{46}$$

where we have introduced the effective particle radius R_2 and the effective membrane thickness ℓ_2 as derived from the stress profiles of an asymmetric bilayer.

F. Spontaneous curvature from stress profile

As shown in our previous study,[3] the spontaneous curvature m can be obtained from the stress profile of a planar bilayer using two different computational methods. First, we can determine the spontaneous curvature m from the first moment of the stress profile using the relation[27]

$$2\kappa m = -\int_{-\infty}^{+\infty} {\rm d}z\; s(z)\, z, \tag{47}$$

provided the membrane is tensionless and $\Sigma^{\rm pl} = 0$. This relation describes the equality between the nanoscopic and the microscopic torque (or bending moment) acting onto a cross section of the bilayer.

Alternatively, we can determine the spontaneous curvature from the leaflet tensions $\Sigma^{\rm pl}_{\rm ex}$ and $\Sigma^{\rm pl}_{\rm in}$. For hard-core interactions, we derived the linear relationship Eq. (26) between the spontaneous curvature m and the tension difference $\Sigma^{\rm pl}_{\rm in} - \Sigma^{\rm pl}_{\rm ex}$ which is equivalent to

$$2\kappa m = \frac{1}{2}\,(\ell_{\rm hw} + R_{\rm hc})(\Sigma^{\rm pl}_{\rm in} - \Sigma^{\rm pl}_{\rm ex}). \tag{48}$$

We will see that the DPD simulations of the soft-core particles are well fitted by the analogous linear relationship

$$2\kappa m = \frac{1}{2}\,(\ell_2 + R_2)(\Sigma^{\rm pl}_{\rm in} - \Sigma^{\rm pl}_{\rm ex}), \tag{49}$$

where we use the same effective membrane thickness ℓ_2 and the same effective particle radius R_2 as in Eq. (46) because the relations (49) and (46) are obtained from the same stress profiles of the asymmetric bilayer. Fitting the simulation data for this stress profile, we obtain the two proportionality factors $R_2(\ell_2 + R_2)$ and $\ell_2 + R_2$ and, thus, both the effective membrane thickness ℓ_2 and the effective particle radius R_2.[28]

IV. SYMMETRIC DEPLETION LAYERS

In this section, we consider single bilayer membranes in a cuboid simulation box. Because of the periodic boundary conditions in the z-direction perpendicular to the membrane, both sides of the membrane are exposed to the same molar concentration, X, of the particles. A typical snapshot of such a membrane is displayed in Fig. 2.

A. Symmetric bilayers with zero bare tension

We first performed DPD simulations of bilayers with projected lipid area $A = A_0 = 1.22\, d^2$. The lateral dimensions of the simulation box were $L_x = L_y = 32\, d$ and the bilayer contained 1678 lipid molecules. The height of the simulation box was varied from $L_z = 32\, d$ to $L_z = 40\, d$ to $L_z = 48\, d$. The number of water beads was adjusted so that the normal pressure was $P_N = 20.7\, k_{\rm B}T/d^3$ at the different box sizes. The latter value of P_N corresponds to the pressure of pure water at the standard DPD conditions[3] with the bulk water density $\rho_W = 3/d^3$. In the absence of the non-adhesive particles, the bilayer was essentially tensionless: the bare tension $\Sigma_{\rm no}$

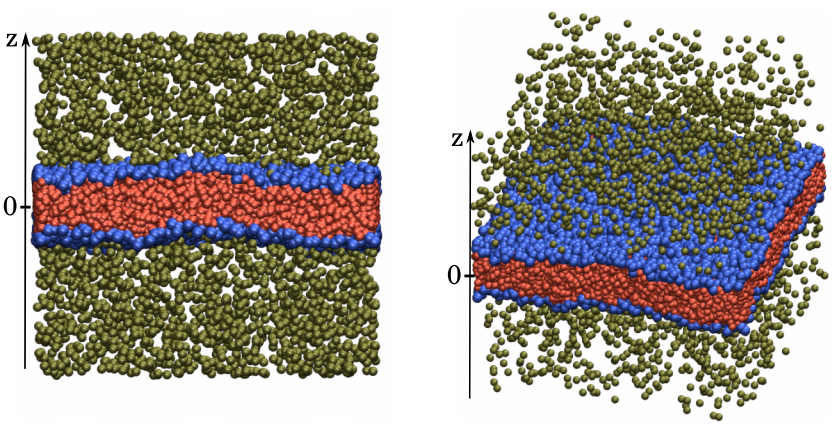

FIG. 2. Simulation snapshots (side and oblique view) of a lipid bilayer exposed to non-adhesive particles. The lipid-head beads (H) and the lipid-chain beads (C) are shown in blue are red, respectively. The non-adhesive beads (P) are shown in tan. The water beads (W) are transparent and not visible. The depletion layers in front of the two leaflets are hardly detectable in the simulation snapshots but can be clearly seen in the ratio of the particle to water densities displayed in Fig. 3(c) below.

had the value $\Sigma_{no} = (0.06 \pm 0.07)\, k_BT/d^2$ and this value was independent of the height of the simulation box.

In the present study, we did not investigate lateral finite size effects, i.e., we did not vary the lateral box size $L_x = L_y$. Such a study has been performed previously in Ref. 29 and revealed a size dependence of the tension of rupture. The lateral size $L_x = L_y = 32\, d$ used here, which is about six times the membrane thickness, was chosen as a compromise between two opposing requirements. On the one hand, we wanted to simulate membrane segments that were large compared to the lateral size of individual lipids in order to study curvature-related properties of the membranes. On the other hand, we also wanted to avoid strong shape fluctuations of the membranes in order to obtain the intrinsic density profiles of the H and C beads across the bilayer. If we simulated much larger membrane patches, these intrinsic profiles would be smeared out by the shape fluctuations and we would need to introduce some deconvolution procedure in order to retrieve the intrinsic profiles from the simulation data.

1. Variation of particle mole fraction

We next performed DPD simulations of the bilayer exposed to the non-adhesive particles. In these simulations, the mole fraction Φ_P of the particles was varied from 0.005 to 0.3, and the normal pressure was kept at the constant level $P_N = 20.7\, k_BT/d^3$ to suppress finite-size effects. The height of the simulation box was varied from $L_z = 32\, d$ to $L_z = 40\, d$ to $L_z = 48\, d$.

Fig. 3 shows the results of simulations for mole fraction $\Phi_P = 0.22$. As mentioned, the normal pressure was adjusted to $P_N = 20.7\, k_BT/d^3$ for all box sizes studied. The bilayer tension is $\Sigma^{pl} = (0.41 \pm 0.07)\, k_BT/d^2$, the latter value being independent of the box height L_z within the statistical error. Note that this tension is substantially larger than the membrane tension in the absence of the non-adhesive particles. As shown in Figs. 3(a) and 3(b), the density profiles $\rho(z)$ for the C, H, W, and P beads were found to be identical for $L_z = 32\, d$, $40\, d$, and $48\, d$. Likewise, we found essentially the same stress profile $s(z)$ for all three values of L_z, see Fig. 3(d). Thus, we did not observe any finite size effects arising from the box height L_z. For comparison, Fig. 3(d) also displays the stress profile $s(z)$ for the symmetric and tensionless state for $\Phi_P = 0$, i.e., in the absence of the particles. The stress profile $s(z)$ displayed in Fig. 3(d) has the same qualitative features as found in previous simulation studies:[3,20,21] Two double-peaks with $s(z) > 0$ for the two head group layers and a pronounced minimum with $s(z) < 0$ for the hydrophobic core of the bilayer.

2. Density profiles and bulk concentration

The number density profiles of the lipid head (H) and chain (C) beads are displayed in Fig. 3(a). The hydrophobic core of the bilayer is characterized by a pronounced maximum in the C density profile. The position of this maximum defines the midplane of the bilayer and, thus, the origin of the

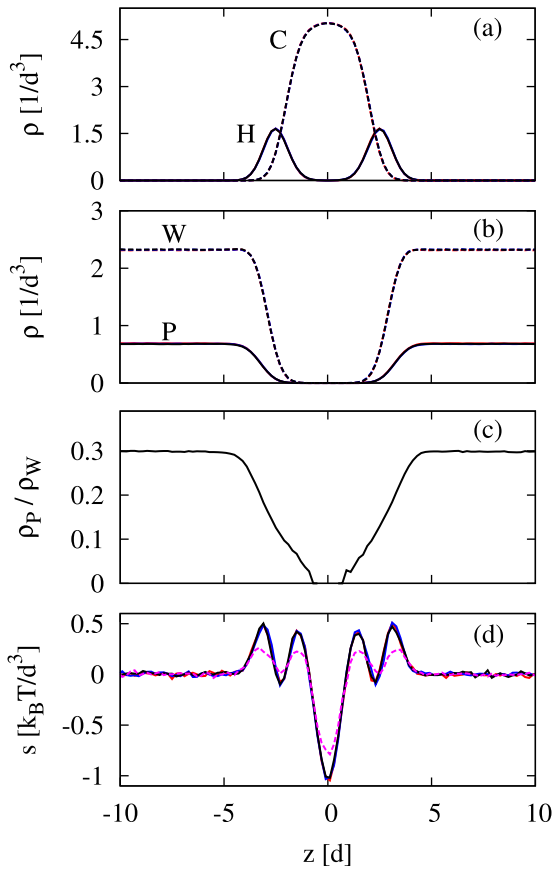

FIG. 3. Simulation data for symmetric bilayers with projected lipid area $A = A_0 = 1.22\, d^2$, particle mole fraction $\Phi_P = 0.22$, and bilayer tension $\Sigma^{pl} = (0.41 \pm 0.07)\, k_BT/d^2$: (a) Number density profiles $\rho(z)$ for C and H beads, (b) number density profiles $\rho_W(z)$ and $\rho_P(z)$ of W and P beads, (c) ratio $\rho_P(z)/\rho_W(z)$ of particle to water densities that directly demonstrates the depletion of the P beads close to the bilayer membrane, and (d) stress profile s as a function of the Cartesian coordinate z perpendicular to the bilayer midplane. In (a), (b), and (d), the red, blue, and black lines correspond to box height $L_z = 32\, d$, $L_z = 40\, d$, and $L_z = 48\, d$, respectively. The congruence of these three lines shows that the density and stress profiles are essentially independent of the box height. The pink dashed line in (d) represents the stress profile for $\Phi_P = 0$, i.e., in the absence of the particles.

z-coordinate perpendicular to the midplane. The H density profile exhibits two smaller peaks, which correspond to the two lipid-water interfaces.

The number density profiles $\rho_W(z)$ and $\rho_P(z)$ of the water (W) and non-adhesive particle (P) beads are shown in Fig. 3(b), the ratio of these two densities, $\rho_P(z)/\rho_W(z)$, is displayed in Fig. 3(c). The water density vanishes within the hydrophobic core of the bilayer, increases gradually at the lipid-water interface, and attains a plateau value further away from the bilayer. The density profile $\rho_P(z)$ of the non-adhesive particles in Fig. 3(b) has a similar shape as the water density profile $\rho_W(z)$ but the density ratio $\rho_P(z)/\rho_W(z)$ in Fig. 3(c) clearly demonstrates that these particles are depleted from the lipid-water interface. The plateau value of the profile $\rho_P(z)$ corresponds to the molar concentration $X = X_{ex} = X_{in}$ of the particles.[30] In what follows, we will discuss our simulation results in terms of the molar concentration X rather than in terms of the mole fraction Φ_P.

3. X-dependence of extended coverage and bilayer tension

The simulation data for the extended coverage $\tilde{\Gamma}^{\rm pl}_{\rm sy}$ as a function of X are displayed in Fig. 4(a), where the red, blue, and black lines correspond to $L_z = 32\,d$, $L_z = 40\,d$, and $L_z = 48\,d$, respectively. The data confirm the linear relationship between $\tilde{\Gamma}^{\rm pl}$ and X in Eq. (37) and lead to the estimate $(\ell_1 + 2R_1)/d = 6.45 \pm 0.02$ for the proportionality factor $\ell_1 + 2R_1$. As shown in Fig. 4(b), the simulations also provide strong evidence that the bilayer tension $\Sigma^{\rm pl}$ of the planar membrane increases linearly with the molar concentration X. We determine the average value of the effective particle radius R_1 from a least-squares fit of the data in Fig. 4(b) to Eq. (43) and estimate the uncertainty of this average value from the band of scattered data that are located between the upper and lower dashed lines in Fig. 4(b). As a result, we obtain the effective particle radius $R_1/d = 0.28 \pm 0.07$.

B. Symmetric bilayers with negative bare tension

We also studied symmetric bilayers with projected area per lipid $A = 1.20\,d^2 < A_0$. In the absence of the particles, we measured the negative bare tension $\Sigma_{\rm no}$

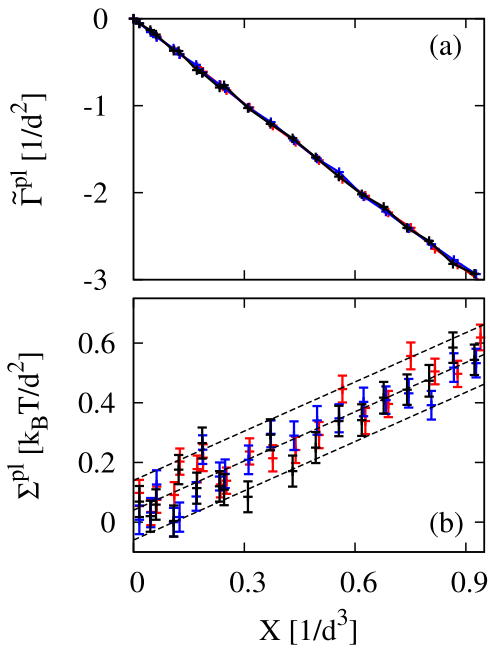

FIG. 4. Extended coverage $\tilde{\Gamma}^{\rm pl} = \tilde{\Gamma}^{\rm pl}_{\rm sy}$ and bilayer tension $\Sigma^{\rm pl}$ as a function of particle concentration X for symmetric bilayers with projected lipid area $A = A_0 = 1.22\,d^2$ and bare tension $\Sigma_{\rm no} = (0.06 \pm 0.07)\,k_{\rm B}T/d^2$. (a) Extended coverage $\tilde{\Gamma}^{\rm pl} = \tilde{\Gamma}^{\rm pl}_{\rm sy}$ versus particle concentration X as computed via Eq. (35). The data are very well described by the linear relation (37) corresponding to a straight line with slope $-\frac{1}{2}(\ell_1 + 2R_1)$; a least-squares fit leads to $(\ell_1 + 2R_1)/d = 6.45 \pm 0.02$; (b) X-dependence of the bilayer tension $\Sigma^{\rm pl}$. In the absence of the particles, i.e., for $X = 0$, the bilayer is tensionless. The data are consistent with the linear X-dependence as given by Eq. (43). A least-squares fit of the data to the latter equation leads to the intermediate dashed line with slope $\langle R_1 \rangle/d = 0.28$ corresponding to the average value of R_1. The uncertainty of this value is obtained from the band of scattered data that are located between the upper and the lower dashed lines, both of which have the same slope $\langle R_1 \rangle/d = 0.28$. As a result, we find $R_1/d = 0.28 \pm 0.07$ for the effective particle radius R_1. The red, blue and black data correspond to $L_z = 32\,d$, $L_z = 40\,d$, and $L_z = 48\,d$, respectively.

$= (-0.31 \pm 0.07)\,k_{\rm B}T/d^2$, corresponding to a slightly compressed membrane. We then added the non-adhesive particles and varied their bulk concentration from 0 to about $1.6/d^3$. The corresponding simulation data are displayed in Fig. 5. The simulations were again carried out in a cubic box with dimensions $L_x = L_y = L_z = 32\,d$ and the number of the water beads was again adjusted to keep the normal pressure constant, $P_N = 20.7\,k_{\rm B}T/d^3$ for all X-values.

1. X-dependence of extended coverage and bilayer tension

The simulation data for the extended coverage $\tilde{\Gamma}^{\rm pl}_{\rm sy}$ on a single leaflet of a symmetric bilayer are displayed in Fig. 5(a) as a function of X. The data confirm the linear relationship between $\tilde{\Gamma}^{\rm pl}_{\rm sy}$ and X in Eq. (37) and lead to the estimate $(\ell_1 + 2R_1)/d = 6.47 \pm 0.01$ for the proportionality factor $\ell_1 + 2R_1$. As shown in Fig. 5(b), the simulations also provide strong evidence that the bilayer tension $\Sigma^{\rm pl}$ of the planar membrane increases linearly with the molar concentration X. We again determine the average value of R_1 from a least-squares fit of the data in Fig. 5(b) to the linear relation (43) and estimate the uncertainty of this value from the band of scattered data between the upper and lower dashed lines as explained before. As a result, we obtain the value $R_1/d = 0.27 \pm 0.07$ for the effective particle radius R_1. Furthermore, inspection of Fig. 5(b) also reveals that the membrane becomes tensionless for particle concentration $X = X_0 = (0.72 \pm 0.18)/d^3$.

2. Particle density and stress profiles

The particle density profiles $\rho_{\rm P}(z)$ in Fig. 5(c) demonstrate that the non-adhesive particles are effectively repelled from the membrane. Indeed, inspection of Fig. 5(c) shows that the particle density profiles $\rho_{\rm P}(z)$ vanish close to the density peaks of the head group beads, irrespective of the bulk concentration X of the particles. The effect of the particle-membrane repulsion on the lateral stress profile $s(z)$ is shown in Fig. 5(d). Inspection of the latter plot shows that the outer peaks of the stress profile grow with increasing particle concentration. These outer peaks are localized around the interfaces between the head groups and the particle solution whereas the inner peaks are at the interfaces between the head groups and the hydrocarbon chains. The outer peaks should increase with the particle concentration because of the growing number of interactions between the P and the H beads. On the other hand, the inner peaks should be only weakly affected by changes in the particle concentration because the particles do not penetrate into the head group layer.

V. ASYMMETRIC DEPLETION LAYERS

A. Simulation setup

To investigate the spontaneous curvature induced by asymmetric depletion layers, we need to impose two different particle concentrations, $X_{\rm in}$ and $X_{\rm ex}$, on the two sides of a bilayer membrane. Because of the periodic boundary condition

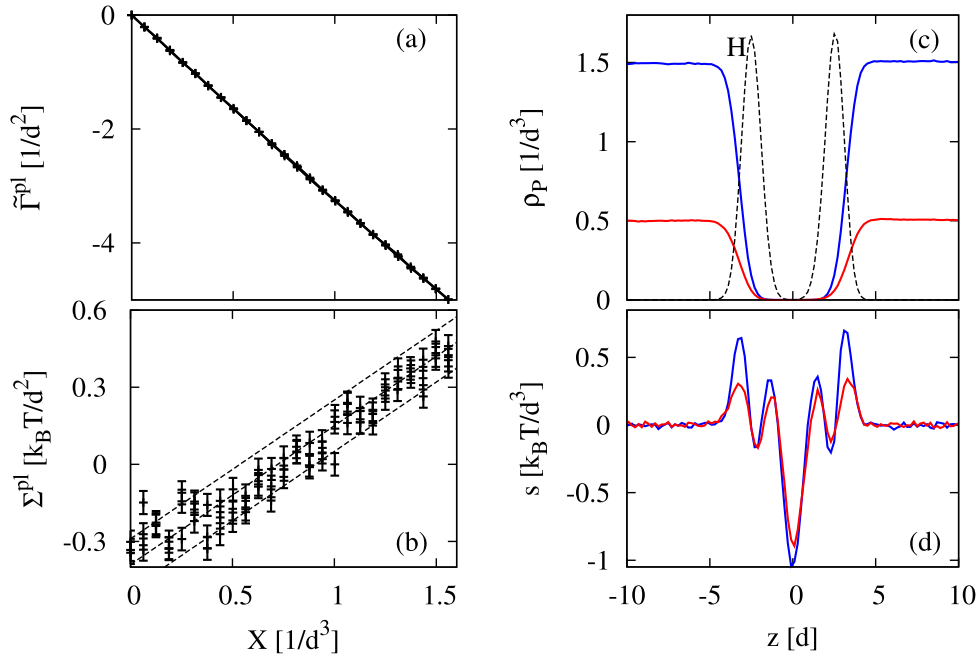

FIG. 5. Simulation data for symmetric bilayers with projected lipid area $A = 1.2\,d^2 < A_0$ and negative bare tension $\Sigma_{no} = (-0.31 \pm 0.07)\,k_BT/d^2$: (a) Extended coverage $\tilde{\Gamma}^{pl} = \tilde{\Gamma}^{pl}_{sy}$ on a single leaflet versus particle concentration X. The data are very well described by the linear relation (37) corresponding to a straight line with slope $-\frac{1}{2}(\ell_1 + 2R_1)$; a least-squares fit leads to $(\ell_1 + 2R_1)/d = 6.47 \pm 0.01$; (b) bilayer tension Σ^{pl} as a function of X. The tension vanishes for particle concentration $X = X_0 = (0.72 \pm 0.18)/d^3$. The data for the tension are consistent with the linear X-dependence as given by Eq. (44). Using the same fitting procedure as for the data in Fig. 4(b), we obtain the estimate $R_1/d = 0.27 \pm 0.07$ for the effective particle radius R_1. The dashed lines have the slope $2R_1/d = 0.54$; (c) particle density profiles $\rho_P(z)$, and (d) stress profile $s(z)$ for bulk concentrations $X = 0.5/d^3$ (red lines) and $X = 1.5/d^3$ (blue lines). The black dashed line in (c) corresponds to the density profile $\rho_H(z)$ of the head beads. The simulation box had the dimensions $L_x = L_y = L_z = 32\,d$.

in the z-direction, we then need to simulate two bilayers as in Fig. 6. As shown in this figure, one bilayer is located at $z > 0$ and the other at $z < 0$. The "upper" bilayer at $z > 0$ is denoted by $\mathcal{B}^{upp}$, the "lower" bilayer at $z < 0$ by $\mathcal{B}^{low}$. The two bilayers are, on average, parallel and partition the simulation box into two compartments which have the same volume. The same geometry was previously used in order to study the spontaneous curvature arising from asymmetric adsorption layers.[3]

In the DPD simulations, the projected area per lipid was $A = 1.20\,d^2 < A_0$ for each bilayer. As explained in Sec. IV B, the two bilayers then experience the negative tension $\Sigma_{no} = (-0.31 \pm 0.07)\,k_BT/d^2$ in the absence of the particles, see Fig. 5(b). The simulation box was now elongated in the z-direction and had the dimensions $L_x = L_y = 32\,d$ and $L_z = 64\,d$. For any pair of concentrations, X_{in} and X_{ex}, the number of water beads was adjusted to keep the normal pressure constant at the selected value $P_N = 20.7\,k_BT/d^3$.

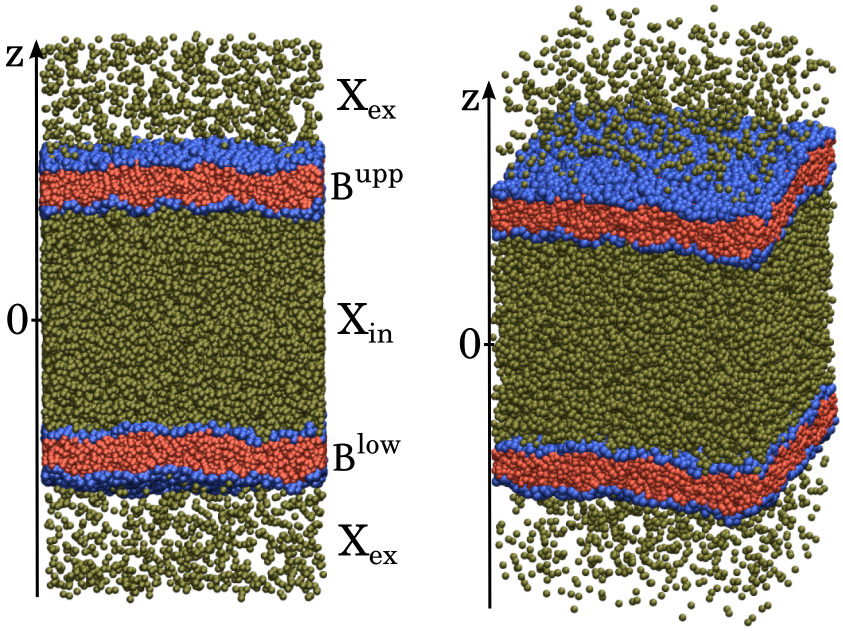

FIG. 6. Simulation snapshots (side and oblique view) of two lipid bilayers, $\mathcal{B}^{upp}$ and $\mathcal{B}^{low}$, that partition the simulation box into two equal subvolumes. The upper leaflet of $\mathcal{B}^{low}$ and the lower leaflet of $\mathcal{B}^{upp}$ are exposed to the particle concentration X_{in}. Likewise, the lower leaflet of $\mathcal{B}^{low}$ and the upper leaflet of $\mathcal{B}^{upp}$ are exposed to the particle concentration $X_{ex} < X_{in}$. The color code is the same as in Fig. 2.

The numbers of particles were conserved in each of the two compartments for all simulation runs, i.e., the particles did not cross the bilayers on the time scale of several microseconds.

B. Asymmetric and tensionless membranes

For the hard-core system, asymmetric and tensionless membranes were obtained for pairs of particle concentrations, $X_{\rm in}$ and $X_{\rm ex}$, with $\frac{1}{2}\,(X_{\rm in}+X_{\rm ex})=X_0$, see Eq. (31), where X_0 is the particle concentration at which the symmetric membrane becomes tensionless, for the same tension $\Sigma_{\rm no}$ of the bare membrane in the absence of particles. For the soft-core system studied by simulations, we find the analogous relationship

$$\frac{1}{2}\,(X_{\rm in}+X_{\rm ex})=X_0 \quad \text{with } X_0\,d^3=0.72\pm0.18 \tag{50}$$

as determined in Sec. IV B, see Fig. 5. The pairs of concentrations $X_{\rm in}$ and $X_{\rm ex}$ for which both bilayers are found to be practically tensionless, i.e., for which both $|\Sigma^{\rm upp}|<0.07\,k_{\rm B}T$ and $|\Sigma^{\rm low}|<0.07\,k_{\rm B}T$, are shown in Fig. 7(a). For all these concentration pairs we obtain density and stress profiles as shown in Fig. 8 for $X_{\rm in}=1.13/d^3$ and $X_{\rm ex}=0.31/d^3$ with $\frac{1}{2}\,(X_{\rm in}+X_{\rm ex})=0.72/d^3$.

The bilayers acquire a spontaneous curvature as soon as their two leaflets are exposed to different concentrations of the non-adhesive particles. We define the concentration difference ΔX by

$$\Delta X\equiv X_{\rm ex}-X_{\rm in} \quad \text{for bilayer} \quad \mathcal{B}^{\rm upp} \tag{51}$$

and

$$\Delta X\equiv X_{\rm in}-X_{\rm ex} \quad \text{for bilayer} \quad \mathcal{B}^{\rm low}. \tag{52}$$

Because we take $X_{\rm in}>X_{\rm ex}$ in our simulations, $\Delta X<0$ for the upper bilayer and $\Delta X>0$ for the lower bilayer.

Fig. 7(b) displays the bilayer tension $\Sigma^{\rm pl}$ as a function of the concentration difference ΔX. The data points for negative values of ΔX correspond to the tension within the upper bilayer, $\Sigma^{\rm upp}$, and the data points for positive values of ΔX correspond to the tension within the lower bilayer, $\Sigma^{\rm low}$. Inspection of Fig. 7(b) shows that all membranes are tensionless with $|\Sigma^{\rm upp}|<0.07\,k_{\rm B}T$ and $|\Sigma^{\rm low}_{\rm mec}|<0.07\,k_{\rm B}T$ for all the data points.

C. Spontaneous curvature

Generalizing Eq. (47) to the two asymmetric and tensionless bilayers displayed in Fig. 6, we obtain the relation

$$2\kappa m^{\rm upp}=-\int_0^{+L_z/2}{\rm d}z\;z\;s(z) \tag{53}$$

for the spontaneous curvature $m^{\rm upp}$ of the upper bilayer and the relation

$$2\kappa m^{\rm low}=-\int_{-L_z/2}^{0}{\rm d}z\;z\;s(z) \tag{54}$$

for the spontaneous curvature $m^{\rm low}$ of the lower bilayer. As shown in Fig. 7(c), the calculated values of these spontaneous curvatures decrease linearly with increasing concentration

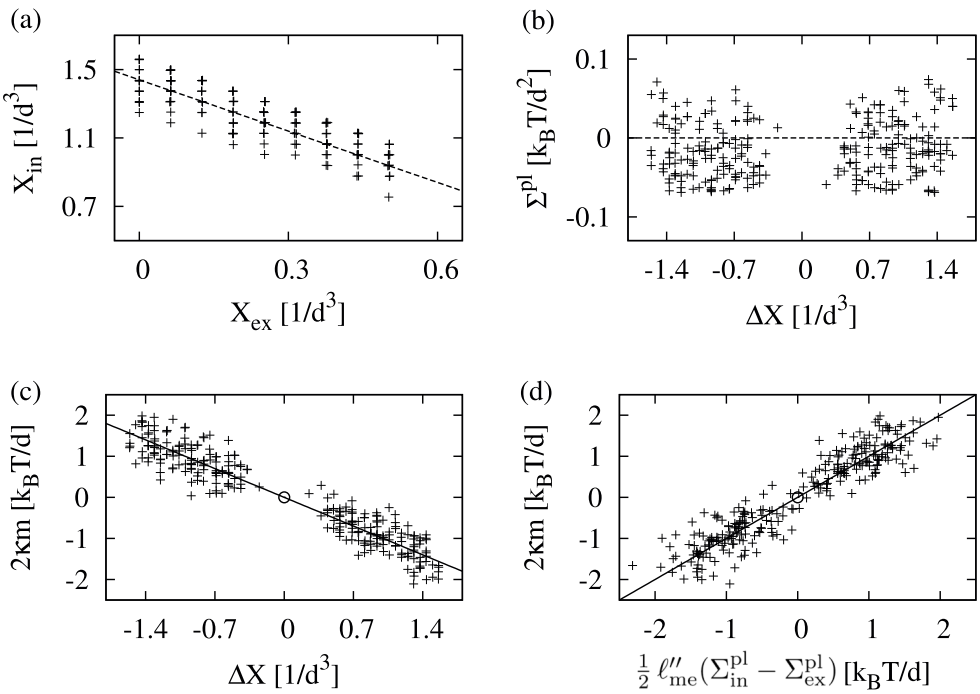

FIG. 7. Spontaneous curvature of bilayer membranes arising from asymmetric depletion layers: (a) Pairs of particle concentrations, $X_{\rm in}$ and $X_{\rm ex}$, in the interior and exterior compartments for which both bilayers are (almost) tensionless. The dashed line corresponds to $X_{\rm in}+X_{\rm ex}=2X_0$ with $X_0=0.72/d^3$ as deduced from the data in Fig. 5(b), (b) bilayer tension $\Sigma^{\rm pl}$ as a function of the concentration difference ΔX. The data points for $\Delta X<0$ and $\Delta X>0$ correspond to the upper and lower bilayer in Fig. 6, respectively, see Eqs. (51) and (52), (c) spontaneous curvature m as obtained from Eqs. (53) and (54) as a function of the concentration difference ΔX. The linear relation between $2\kappa m$ and ΔX is consistent with Eq. (46); the solid line corresponds to a fit with $R_2(\ell_2+R_2)=2\,d^2$, and (d) spontaneous curvature $2\kappa m$ as in (c) plotted against the parameter combination $\frac{1}{2}\,\ell''_{\rm me}(\Sigma^{\rm pl}_{\rm in}-\Sigma^{\rm pl}_{\rm ex})$ as in Eq. (49) with $\ell''_{\rm me}\equiv\ell_2+R_2=6\,d$. The solid line corresponds to the identity of these two quantities.

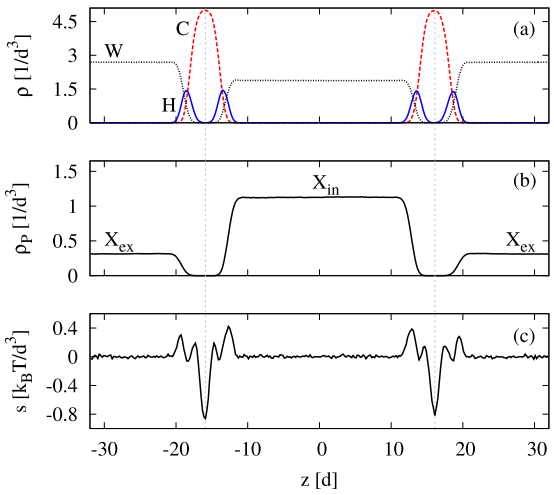

FIG. 8. ((a) and (b)) Density profiles and (c) stress profile of two parallel bilayers as a function of the coordinate z perpendicular to the bilayers. The projected lipid area is $A = 1.20\,d^2$ for each bilayer. The particles have the concentrations $X_{\rm in} = 1.13/d^3$ and $X_{\rm ex} = 0.31/d^3$ in the interior and exterior compartment, respectively. The dimensions of the simulation box are $L_x = L_y = 32d$ and $L_z = 64d$. The number of the water beads is adjusted so that the normal pressure $P_N = 20.7\,k_{\rm B}T/d^3$. (a) The density profiles of the C, H, and W beads, (b) the density profile $\rho_P(z)$ of the particles. The concentrations $X_{\rm in}$ and $X_{\rm ex}$ are chosen in such a way that the membranes experience (almost) no mechanical tension, and (c) the lateral stress profile $s(z)$ of the two tensionless membranes.

difference ΔX. Our definition of this difference implies that the data points with negative ΔX-values correspond to the upper bilayer $\mathcal{B}^{\rm upp}$ with $m = m^{\rm upp} > 0$ while the data points with positive ΔX-values correspond to the lower membrane $\mathcal{B}^{\rm low}$ with $m = m^{\rm low} < 0$.

The simulation data in Fig. 7(c) are consistent with the relation (46) which was proposed in analogy to the exact relation (19) for the hard-core system in Sec. II. Because of the noisy data for $2\kappa m$, the proportionality factor $R_2(\ell_2 + R_2)$ in Eq. (46) has a relatively large uncertainty. A least-squares fit for the average value of this prefactor together with a conservative estimate for its uncertainty leads to $R_2(\ell_2 + R_2)/d^2 = 2 \pm 0.6$. Likewise, the simulation data in Fig. 7(d) confirm the relation (49) which is analogous to the exact relation (26) for the hard-core system. The numerical value for the proportionality factor $\ell_2 + R_2$ is estimated to be $(\ell_2 + R_2)/d = 6 \pm 2$.

VI. DISCUSSION OF SIMULATION RESULTS

A. Linear relationships and associated length scales

As described in Secs. IV and V, our simulation data provide several linear relationships between different quantities of interest. First, for symmetric bilayers, the data in Figs. 4 and 5 confirm the linear dependencies of the extended coverage $\tilde{\Gamma}^{\rm pl}_{\rm sy}$ and of the bilayer tension $\Sigma^{\rm pl}$ on the molar concentration X as described by Eqs. (37) and (43), which were proposed in close analogy to the hard-core equations (36) and (18). Second, for asymmetric bilayers, the data in Fig. 7 corroborate the linear dependencies of the spontaneous curvature m on the concentration difference ΔX and on the difference $\Sigma^{\rm pl}_{\rm in} - \Sigma^{\rm pl}_{\rm ex}$ of the leaflet tensions as described by Eqs. (46) and (49).

The data for the extended coverage $\tilde{\Gamma}^{\rm pl}_{\rm sy}$ are obtained from the particle density profile $\rho_P(z)$ which can be simulated with high accuracy. In contrast, the bilayer tension $\Sigma^{\rm pl}$ and the spontaneous curvature m as well as the leaflet tensions $\Sigma^{\rm pl}_l$ are obtained from the symmetric and asymmetric stress profiles, which are less accurate. As a consequence, the data for $\tilde{\Gamma}^{\rm pl}_{\rm sy}$ in Figs. 4(a) and 5(a) have very small error bars whereas the other data are rather noisy, see Figs. 4(b) and 5(b), as well as Figs. 7(b)–7(d).

The proportionality factors for the linear relationships have been denoted by $\ell_1 + 2R_1$, R_1, $R_2(\ell_2 + R_2)$, and $\ell_2 + R_2$ as defined by Eqs. (37), (43), (46), and (49) and were introduced in close analogy to the hard-core system. These four proportionality factors contain four length scales, the effective membrane thicknesses ℓ_1 and ℓ_2 as well as the effective particle radii R_1 and R_2 which we have distinguished because they should, in general, depend on the details of the different density and stress profiles from which they are derived. In order to reduce the number of relevant length scales, it would be desirable to identify the effective membrane thicknesses ℓ_1 and ℓ_2 as well as the effective particle radii R_1 and R_2. We will now examine whether such an identification is consistent with the simulation data.

From the data in Figs. 7(c) and 7(d), which are derived from the asymmetric stress profiles, the proportionality factors were found to be $R_2(\ell_2 + R_2) = 2d^2$ and $\ell_2 + R_2 = 6d$ with an accuracy of about 30%. A combination of these two equations leads to the estimates $R_2/d = 0.33 \pm 0.1$ and $\ell_2/d = 5.67 \pm 1.9$ for the effective particle radius R_2 and the effective membrane thickness ℓ_2. Likewise, from the simulation data displayed in Figs. 5(a) and 5(b), we obtain the proportionality factors $(\ell_1 + 2R_1)/d = 6.47 \pm 0.01$ and $R_1/d = 0.27 \pm 0.07$ which leads to the effective membrane thickness $\ell_1/d = 5.93 \pm 0.08$.

We thus conclude that the membrane thicknesses ℓ_1 and ℓ_2 as well as the particle radii R_1 and R_2 are approximately equal and can be identified within the accuracy of our simulation data. However, based on these data, we cannot exclude the possibility that these length scales are somewhat different reflecting the details of the different particle density and stress profiles from which they have been derived. Furthermore, these length scales are expected to depend, in general, on the chosen set of DPD parameters. In contrast, the linear dependencies of the extended coverages and the bilayer tension on the molar concentration X as well as the linear relationship between the spontaneous curvature and the concentration difference ΔX should be universal and independent of the DPD parameters.

B. Concentration regimes

The linear relationships discussed in Subsection VI A are observed in the simulations over a relatively large concentration range. Indeed, for symmetric bilayers, the linear dependence of the extended coverage and of the bilayer tension on the molar concentration X is observed over the range $0 < X \leq 1.5/d^3$ as shown in Fig. 5. Likewise, for asymmetric

bilayers, the linear dependence of the spontaneous curvature on the concentration difference ΔX is observed over the range $-1.5/d^3 \leq \Delta X \leq 1.5/d^3$ as displayed in Fig. 7.

Because the total bead density has the essentially constant value $3/d^3$ at constant pressure, the simulation box contains about the same number of particle and water beads for the largest particle concentration $X = 1.5/d^3$ which thus corresponds to a concentrated solution in which the volume fraction of the particle beads is close to 0.5. It is quite remarkable that the linear relationships are found to apply for such high particle concentrations because these relationships were originally derived for an ideal gas of spherical particles that experience no mutual interactions but only hard-core interactions with the membrane. As explained in Sec. II E, the ideal-gas description should provide a reliable approximation for a dilute solution of hard spheres with diameter $d_{\rm hc}$ provided the molar concentration X is sufficiently small and satisfies $X < X_o = 0.478/d_{\rm hc}^3$ as in Eq. (21). In contrast, for the soft-spheres with diameter d as studied in our simulations, the linear relationships apply to much larger concentrations up to $X = 1.5/d^3$.

VII. SUMMARY AND OUTLOOK

In summary, we first considered a hard-core system consisting of an ideal gas of hard-core particles of radius $R_{\rm hc}$ interacting with a "hard wall" membrane of thickness $\ell_{\rm hw}$. For this system, we analytically calculated the dependencies of the leaflet coverages and leaflet tensions on the particle concentrations. For a planar membrane, both dependencies are linear as described by the relationships in Eqs. (8)-(10). The solution of the hard-core system also shows explicitly that we can calculate the spontaneous curvature m as given by Eq. (19) from the properties of the planar membrane, see Eqs. (25) and (26). Depending on the particle size, the particle concentrations, and the membrane's bending rigidity, the magnitude of the depletion-induced spontaneous curvature can be fairly large, see Table I.

Linear relationships analogous to those derived for the hard-core system were also obtained for the soft-core particles studied by DPD simulations. In particular, we found linear relationships (i) between the membrane tension $\Sigma^{\rm pl}$ of symmetric bilayers and the particle concentration X (Eq. (44) and Fig. 5(b)) and (ii) between the spontaneous curvature m and the difference ΔX of the particle concentrations on the two sides of the membrane (Eq. (46) and Fig. 7(c)). In this way, our results provide strong evidence that the linear dependencies (i) and (ii) are universal in the sense that they do not depend on the nature of the interparticle interactions, in contrast to the prefactors of these relationships which are expected to reflect the interaction parameters.

The simulation results reported here scrutinize and corroborate the analytical theory introduced in Ref. 1 which focussed on the loss of *translational* entropy. Other theoretical studies considered rod-like particles and examined the loss of *configurational* entropy when these rods come close to a membrane.[18,19] The latter entropy loss was found to contribute to the second but not to the first order in the membrane's mean curvature, i.e., the results of Refs. 18 and 19 imply that the configurational entropy loss of rod-like particles does not contribute to the spontaneous curvature of the membrane. However, rod-like particles close to a membrane also suffer a loss of translational entropy which will again contribute to the membrane's spontaneous curvature.

The membranes considered in this paper are lipid bilayers which typically have a bending rigidity of the order of $20\,k_{\rm B}T$. Because the bending rigidity provides the basic energy scale for the membranes, our study explores the low-temperature regime in which shape fluctuations or bending undulations are expected to play only a minor role. The opposite case has been investigated theoretically in Ref. 31 and it was proposed that strong shape fluctuations lead to a constant density profile of the particles adjacent to a fluctuating membrane. The latter proposal has not been addressed here and remains to be corroborated by molecular simulations.

Our theoretical results can be scrutinized by systematic experimental studies. Indeed, a large variety of nanoparticles could be used in order to study the depletion effects described here. The smallest "particles" are monoatomic ions which form exclusion layers in front of the bilayer leaflets, with a thickness of up to 1 nm.[13] Somewhat larger particles are water-soluble macromolecules such as short PEG chains[15] or small sugar molecules.[14,32] In fact, even adhesive nanoparticles experience effectively repulsive interactions with lipid membranes when the size of the particles is below a certain critical size.[33] In all of these cases, the spontaneous curvature induced by asymmetric depletion layers can be measured via the spontaneous tabulation of giant vesicles.[34]

ACKNOWLEDGMENTS

B.R. has been supported by the Polish Ministry of Science and Higher Education via Grant No. IP2012 0383 72.

[1]R. Lipowsky and H. G. Döbereiner, "Vesicles in contact with nanoparticles and colloids," Europhys. Lett. **43**, 219–225 (1998).
[2]H. Terasawa, K. Nishimura, H. Suzuki, T. Matsuura, and T. Yomo, "Coupling of the fusion and budding of giant phospholipid vesicles containing macromolecules," Proc. Natl. Acad. Sci. U. S. A. **109**, 5942–5947 (2012).
[3]B. Różycki and R. Lipowsky, "Spontaneous curvature of bilayer membranes from molecular simulations: Asymmetric lipid densities and asymmetric adsorption," J. Chem. Phys. **142**, 054101 (2015).
[4]S. Asakura and F. Oosawa, "Interaction of particles suspended in solutions of macromolecules," J. Polym. Sci. **33**, 183–192 (1958).
[5]C. Sieglaff, "Phase separation in mixed polymer solutions," J. Polym. Sci. **4**, 319–326 (1959).
[6]H. N. W. Lekkerkerker, C.-K. Poon, N. Pusey, A. Stoobants, and P. B. Warren, "Phase behaviour of colloid + polymer mixtures," Europhys. Lett. **20**, 559–564 (1992).
[7]E. Eisenriegler, A. Hanke, and S. Dietrich, "Polymers interacting with spherical and rodlike particles," Phys. Rev. E **54**, 1134–1152 (1996).
[8]M. Dijkstra, R. van Roij, and R. Evans, "Phase diagram of highly asymmetric binary hard-sphere mixtures," Phys. Rev. E **59**, 5744–5771 (1999).
[9]A. Hanke, E. Eisenriegler, and S. Dietrich, "Polymer depletion effects near mesoscopic particles," Phys. Rev. E **59**, 6853–6878 (1999).
[10]A. P. Gast, W. B. Russel, and C. K. Hall, "An experimental and theoretical study of phase transitions in the polystyrene latex and hydroxyethylcellulose system," J. Colloid Interface Sci. **109**, 161–171 (1986).
[11]S. Ramakrishnan, M. Fuchs, K. S. Schweizer, and C. F. Zukoski, "Entropy driven phase transitions in colloid–polymer suspensions: Tests of depletion theories," J. Chem. Phys. **116**, 2201–2212 (2002).

[12]R. Tuinier, J. Rieger, and C. de Kruif, "Depletion-induced phase separation in colloid–polymer mixtures," Adv. Colloid Interface Sci. **103**, 1–31 (2003).
[13]H. I. Petrache, I. Kimchi, D. Harries, and V. A. Parsegian, "Measured depletion of ions at the biomembrane interface," J. Am. Chem. Soc. **127**, 11546–11547 (2005).
[14]P. Westh, "Glucose, sucrose and trehalose are partially excluded from the interface of hydrated DMPC bilayers," Phys. Chem. Chem. Phys. **10**, 4110–4112 (2008).
[15]S. W. Hui, T. L. Kuhl, Y. Q. Guo, and J. Israelachvili, "Use of poly(ethylene glycol) to control cell aggregation and fusion," Colloids Surf., B **14**, 213–222 (1999).
[16]R. Lipowsky, "Bending of membranes by anchored polymers," Europhys. Lett. **30**, 197–202 (1995).
[17]M. Breidenich, R. Netz, and R. Lipowsky, "The influence of non-anchored polymers on the curvature of vesicles," Mol. Phys. **103**, 3160–3183 (2005).
[18]K. Yaman, M. Jeng, P. Pincus, C. Jeppesen, and C. M. Marques, "Rods near curved surfaces and in curved boxes," Phys. A **247**, 159–182 (1997).
[19]K. Yaman, P. Pincus, and C. Marques, "Membranes in rod solutions: A system with spontaneously broken symmetry," Phys. Rev. Lett. **78**, 4514–4517 (1997).
[20]R. Goetz and R. Lipowsky, "Computer simulations of bilayer membranes: Self-assembly and interfacial tension," J. Chem. Phys. **108**, 7397–7409 (1998).
[21]J. C. Shillcock and R. Lipowsky, "Equilibrium structure and lateral stress distribution of amphiphilic bilayers from dissipative particle dynamics simulations," J. Chem. Phys. **117**, 5048–5061 (2002).
[22]W. Helfrich, "Elastic properties of lipid bilayers: Theory and possible experiments," Z. Naturforsch. **28c**, 693–703 (1973).
[23]U. Seifert, K. Berndl, and R. Lipowsky, "Shape transformations of vesicles: Phase diagram for spontaneous curvature and bilayer coupling model," Phys. Rev. A **44**, 1182–1202 (1991).
[24]M. D. Rintoul and S. Torquato, "Computer simulations of dense hard-sphere systems," J. Chem. Phys. **105**, 9258–9265 (1996).
[25]R. Groot and P. Warren, "Dissipative particle dynamics: Bridging the gap between atomistic and mesoscopic simulation," J. Chem. Phys. **107**, 4423–4435 (1997).
[26]In Ref. 3, the bilayer tension $\Sigma^{\rm pl}$ was denoted by $\Sigma_{\rm mec}$.
[27]W. Helfrich, "Amphiphilic mesophases made of defects," in *Physics of Defects*, edited by R. Balian *et al.* (North-Holland Publishing Company, Amsterdam, 1981), pp. 715–755.
[28]For the hard-core system, we also have the linear relationship $2\kappa m = \frac{1}{2} k_{\rm B}T(\ell_{\rm hw} + R_{\rm hc})(\Gamma^{\rm pl}_{\rm ex} - \Gamma^{\rm pl}_{\rm in})$ between the spontaneous curvature and the difference $\Gamma^{\rm pl}_{\rm ex} - \Gamma^{\rm pl}_{\rm in}$ of the particle coverages on the two leaflets as follows from a combination of (26) and (7). However, this linear relation becomes less transparent when expressed in terms of the extended coverages $\tilde{\Gamma}^{\rm pl}_l$ which are directly accessible to the simulations.
[29]L. Gao, J. Shillcock, and R. Lipowsky, "Improved dissipative particle dynamics simulations of lipid bilayers," J. Chem. Phys. **126**, 015101 (2007).
[30]In Ref. 3, the molar concentration X of the particles was denoted by C.
[31]T. Bickel, M. Benhamou, and H. Kaidi, "Statistical mechanics of a colloidal suspension in contact with a fluctuating membrane," Phys. Rev. E **70**, 051404 (2004).
[32]H. D. Andersen, C. Wang, L. Arlethc, G. H. Peters, and P. Westh, "Reconciliation of opposing views on membrane–sugar interactions," Proc. Natl. Acad. Sci. U. S. A. **108**, 1874–1878 (2011).
[33]J. Agudo-Canalejo and R. Lipowsky, "Critical particle sizes for the engulfment of nanoparticles by membranes and vesicles with bilayer asymmetry," ACS Nano **9**, 3704–3720 (2015).
[34]Y. Liu, J. Agudo-Canalejo, A. Grafmüller, R. Dimova, and R. Lipowsky, "Patterns of flexible nanotubes formed by liquid-ordered and liquid-disordered membranes," ACS Nano **10**, 463–474 (2016).